

Effective g factor in black phosphorus thin films

Xiaoying Zhou,¹ Wen-Kai Lou,^{1,*} Dong Zhang,¹ Fang Cheng,² Guanghui Zhou,³ and Kai Chang^{1,†}

¹*SKLSM, Institute of Semiconductors, Chinese Academy of Sciences, P.O. Box 912, Beijing 100083, China*

²*Department of Physics and Electronic Science, Changsha University and Technology, Changsha 410004, China*

³*Department of Physics and Key Laboratory for Low-Dimensional Quantum Structures and Manipulation (Ministry of Education), and Synergetic Innovation Center for Quantum Effects and Applications of Hunan, Hunan Normal University, Changsha 410081, China*

(Received 28 October 2016; revised manuscript received 12 December 2016; published 9 January 2017)

We theoretically investigate the effective g factor in the black phosphorus (BP) thin films (TFs) based on a multiband $\mathbf{k} \cdot \mathbf{p}$ theory. We demonstrate that the effective single particle g factor in pristine BP TF is anisotropic arising from its anisotropic band structure with $g_{xx}^* \approx g_{yy}^* \approx 2.0$ and g_{zz}^* sensitively depending on the interband coupling and the band gap. The g_{zz}^* approaches 2.0 with increasing hole doping density and gate electric field since both of them diminish the interband coupling by reducing the overlap integral between the electron and hole wave functions. We also estimate the exchange interaction enhancement on the effective single particle g factor by using the screened Hartree-Fock approximation. The exchange interaction enhanced g factor (g_{ex}) shows maxima (minima) at odd (even) filling factors. The effective g factor (g^*) oscillates with the increase of magnetic field and sensitively depends on the Landau level broadening as well as the gate electric field since both of them affect the interband coupling and the electron-electron interactions.

DOI: [10.1103/PhysRevB.95.045408](https://doi.org/10.1103/PhysRevB.95.045408)

I. INTRODUCTION

Black phosphorus (BP) is a two-dimensional (2D) layered material with the atomic layers coupled by van der Waals interactions [1–4]. It is the most stable phase among several allotropes of the group V element phosphorus under normal conditions [5]. Recently, few layer BPs attracted intensive attention due to its unique electronic properties and potential applications in nanoelectronics [1–4,6–10]. Inside each layer, phosphorus atoms are covalently bonded with three adjacent atoms to form a puckered honeycomb structure due to the sp^3 hybridization [1,4]. BP in its bulk form possesses a direct band gap 0.3 eV located at Z point [1,2,7–9,11]. This direct band gap moves to the Γ point in few layer BPs and increases to 2.0 eV when the thickness decreases to monolayer [4,11–13]. Therefore, BP is an appealing candidate for a tunable photodetector from the visible to the infrared part of the electromagnetic spectrum [14,15]. Furthermore, the field-effect transistor based on few layer BP is found to have an on/off ratio of 10^5 and a carrier mobility at room temperature as high as 10^3 cm²/V s [1–3,6], which make BP a favorable material for the next generation electronics.

The low energy dispersion of bulk BP around Z point can be well described by an anisotropic two-band $\mathbf{k} \cdot \mathbf{p}$ Hamiltonian [16,17]. One can obtain the low-energy Hamiltonian for BP thin films (TFs) by applying a confinement in the perpendicular z direction. To date, various interesting properties for BP TFs have been predicted theoretically and verified experimentally, particularly those related to the strain induced gap modification [4], tunable optical properties [18], layer controlled anisotropic excitons [13,19], anisotropic Landau levels (LLs) [20], anomalous magneto-optical properties [21,22], quantum Hall effect [23], and quantum oscillations [24–29]. However, less attention has been paid to the effective g factor in BP TFs [23]. The effective g factor is defined by the scaling

factor g^* between the external magnetic field B and the spin-splitting energy ($g^* \mu_B B$). It always deviates from 2.0 (the bare Landé g factor g_0 in the vacuum) in conventional semiconductors [30–33] since the spin-orbit coupling and electron-electron interactions can affect the quasiparticle energies and renormalize their energy levels, leading to a correction to the spin-splitting energy and the bare electron g factor. A better knowledge of the effective g factor is important for the understanding of magnetotransport, quantum oscillations, magneto-optical spectra of BP, which is just like what had been done in conventional semiconductors [30–33], i.e., the two-dimensional (2D) electron gas in the interface of GaAs/AlGaAs.

In this work we theoretically investigate the effective g factor in the BP TFs based on a multiband $\mathbf{k} \cdot \mathbf{p}$ theory. We demonstrate that the effective single particle g factor in pristine BP TF is anisotropic arising from its anisotropic band structure with $g_{xx}^* \approx g_{yy}^* \approx 2.0$ and g_{zz}^* sensitively depending on the interband coupling and the band gap. The g_{zz}^* in pristine BP ranges from 2.14 to 2.90 as the BP thickness increases from monolayer to bulk. It approaches 2.0 with increasing hole doping density and gate electric field since both of them diminish the interband coupling by reducing the overlap integral between the electron and hole wave functions. We also estimate the exchange interaction enhancement on the effective single particle g factor by using the screened Hartree-Fock approximation. The exchange interaction enhanced g factor (g_{ex}) shows maxima (minima) at odd (even) filling factors. The effective g factor (g^*) oscillates with the increase of magnetic fields and sensitively depends on the Landau level broadening as well as the gate electric field because both of them affect the interband coupling and electron-electron interaction.

The paper is organized as follows. In Sec. II we calculate the electronic structure of BP TFs self-consistently and the single particle g factor as well as the exchange interaction enhancement on it. In Sec. III we present some numerical examples and discussions on the band structure and g factor of BP TFs. Finally, we summarize our results in Sec. IV.

*wk lou@semi.ac.cn

†kchang@semi.ac.cn

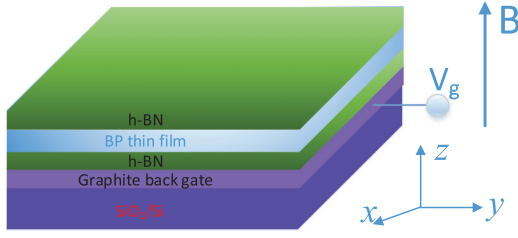


FIG. 1. Schematic illustration of experimental setup on black phosphorus (BP) thin film (TF) structure, which is sandwiched by the hexagonal boron nitride (h-BN) TFs to avoid degeneration. The graphite back gate induces a strong electric field in the BP TF.

II. MODEL AND FORMULISM

A. Electronic structure of BP TFs

In black phosphorus thin films, breaking translation symmetry in the z direction moves the direct gap from the Z point to the Γ point. The low-energy effective Hamiltonian of BP TFs around Γ point can be expressed by $H = H_{\mathbf{k}_{\parallel}} + H_{k_z}$ with its in-plane and out-of-plane dynamics taken separately. The in-plane part is given by [16,17]

$$H_{\mathbf{k}_{\parallel}} = \begin{pmatrix} E_c + \alpha_c k_x^2 + \beta_c k_y^2 & \gamma k_x \\ \gamma k_x & E_v - \alpha_v k_x^2 - \beta_v k_y^2 \end{pmatrix}, \quad (1)$$

where $E_c = 0.15$ eV ($E_v = -0.15$ eV) is the conduction (valence) band edge of bulk BP, $\alpha_{c,v}$ and $\beta_{c,v}$ are related to the effective masses by $\alpha_{(c,v)} = \hbar^2/2m_{(c,v)x}$ and $\beta_{(c,v)} = \hbar^2/2m_{(c,v)y}$ with [16] $m_{cx} = 0.15$, $m_{cy} = 1.07$, $m_{vx} = 0.12$, $m_{vy} = 0.71$, and $\gamma = 2.308$ eV nm describes the interband coupling between conduction and valence band. We take the free electron mass m_0 as the unit of all the effective masses throughout the paper. The out-of-plane Hamiltonian is given by

$$H_{k_z} = \begin{pmatrix} \eta_c k_z^2 & 0 \\ 0 & -\eta_v k_z^2 \end{pmatrix} + eE_z z + V(z), \quad (2)$$

where $\eta_{(c,v)} = \hbar^2/2m_{(c,v)z}$ with $m_{cz} = 0.29$ and $m_{vz} = 0.61$, E_z is the graphite back gate induced electric field (see Fig. 1), and $V(z)$ describes the potential profile in the z direction which consists of the hard wall confining potential at the sample surfaces, and $V_{\text{in}}(z)$ is the internal electrostatic potential caused by charge distribution in the TFs.

For a finite thickness BP with given electric field and $V(z)$, the subbands ϵ_j and the corresponding eigenstates $\varphi_j(z)$ can be obtained numerically by diagonalizing the Schrödinger equation $H_{k_z}(-i\partial_z)\varphi_j(z) = \epsilon_j\varphi_j(z)$, where j is the subband index. On the other hand, the internal electrostatic potential $V_{\text{in}}(z)$ is determined by the Poisson equation

$$\frac{d^2 V_{\text{in}}(z)}{dz^2} = -\frac{[n(z) + p(z) + N_d(z)]}{\epsilon}, \quad (3)$$

where $n(z)$, $p(z)$, and $N_d(z)$ are the densities of electrons, holes, and dopant in the z direction, respectively, and ϵ is the dielectric constant. Meanwhile, $n(z)$ and $p(z)$ can be obtained

from [34,35]

$$n(z) = -|e| \frac{2k_B T}{\pi \hbar^2} \sum_j m_c^{j*} F(E_f - E_c - \epsilon_j^c) |\varphi_j^c(z)|^2, \\ p(z) = |e| \frac{2k_B T}{\pi \hbar^2} \sum_j m_v^{j*} F(E_v + \epsilon_j^v - E_f) |\varphi_j^v(z)|^2, \quad (4)$$

where c and v refer to the conduction band and valence band, respectively, $F(E) = \ln[1 + \exp(E/k_B T)]$ with E_f is the Fermi energy, and m_c^{j*} (m_v^{j*}) refers to the effective mass given by [34] $\sqrt{m_{cx}^{j*} m_{cy}^{j*}}$ ($\sqrt{m_{vx}^{j*} m_{vy}^{j*}}$). Solving the Schrödinger and Poisson equations self-consistently [34,35], we obtain the band structure and corresponding eigenstates of BP TFs.

B. Effective single particle g factor of BP TFs

The effective g factor is defined by the scaling factor g^* between the external magnetic field B and the spin-splitting energy $E_s = g^* \mu_B B$. Armed with the electronic structure of the BP TFs obtained in Sec. II, we now calculate the effective single particle g factor of 2D hole gas in BP TFs based on a multiband $\mathbf{k} \cdot \mathbf{p}$ theory. Within the $\mathbf{k} \cdot \mathbf{p}$ framework, we find that the analytical form of the components for the effective single particle g factor tensor in a crystal is given by

$$g_{\alpha\beta}^* = g_0 \left[\delta_{\alpha\beta} + \frac{1}{im_0} \sum_l \frac{P_{n,l}^\alpha P_{l,n}^\beta - P_{n,l}^\beta P_{l,n}^\alpha}{E_n^{(0)} - E_l^{(0)}} \right], \quad (5)$$

with $\mathbf{P} = \mathbf{p} + \frac{\hbar}{4m_0 c^2} (\boldsymbol{\sigma} \times \nabla V)$, $P_{n,l}^\alpha = \langle n | P_\alpha | l \rangle$, $P_{l,n}^\beta = \langle l | P_\beta | n \rangle$, where $|n\rangle$ is the Bloch state corresponding to the n th Bloch band $E_n^{(0)}$, $g_0 = 2.0$ is the bare Landé g factor in the vacuum. The sum index l runs over all the Bloch bands except the n th. The detail derivation of Eq. (5) is presented in Appendix A. For the effective single particle g factor of the conduction and valence band, we can approximately take the summation in Eq. (5) runs over only Γ_{2v}^+ and Γ_{4c}^- band because only the interband coupling $\langle \Gamma_{4c}^- | p_x | \Gamma_{2v}^+ \rangle$ is dominant among all the symmetry allowed interband couplings related to the conduction and valence band [36]. Therefore, we obtain the effective single particle g factor as

$$g_{xx}^* = g_0 + \frac{g_0}{im_0} \frac{Q_y Q_z^* - Q_z Q_y^*}{E_{\Gamma_{2v}^+}^{(0)} - E_{\Gamma_{4c}^-}^{(0)}}, \\ g_{yy}^* = g_0 + \frac{g_0}{im_0} \frac{Q_z Q_x^* - Q_x Q_z^*}{E_{\Gamma_{2v}^+}^{(0)} - E_{\Gamma_{4c}^-}^{(0)}}, \\ g_{zz}^* = g_0 + \frac{g_0}{im_0} \frac{Q_x Q_y^* - Q_y Q_x^*}{E_{\Gamma_{2v}^+}^{(0)} - E_{\Gamma_{4c}^-}^{(0)}}, \quad (6)$$

with matrix elements $Q_j = \langle \varphi_{2v}^+ | \varphi_{4c}^- \rangle \langle \Gamma_{2v}^+ | P_j | \Gamma_{4c}^- \rangle$ ($j = x, y, z$), where φ is the envelope function obtained in Sec. II A. It has been shown that the dominant components of electron states near Γ point are p_z orbital [4,36,37], $\langle \Gamma_{2v}^+ | P_z | \Gamma_{4c}^- \rangle$ is therefore very small, and can be safely neglected. Hence,

we have

$$g_{xx}^* \simeq g_{yy}^* \simeq 2.0, \quad g_{zz}^* \simeq g_0 \left(1 + \frac{2\alpha_{42} P_{x1} |\langle \varphi_{2v}^+ | \varphi_{4c}^- \rangle|^2}{E_g m_0} \right), \quad (7)$$

where $P_{x1} = \langle \Gamma_{2v}^+ | p_x | \Gamma_{4c}^- \rangle$ are the interband couplings between Γ_{2v}^+ and Γ_{4c}^- , $\alpha_{42} = \frac{i\hbar}{4m_0 c^2} \langle \Gamma_{4c}^- | \partial_x V | \Gamma_{2v}^+ \rangle$ are the parameter related to the spin-orbit coupling in BP, and $\langle \varphi_{2v}^+ | \varphi_{4c}^- \rangle = \langle \varphi_v | \varphi_c \rangle$ is the overlap of the electron and hole wave functions. The parameter P_{x1} can be extracted from the interband coupling as [4] $P_{x1} = \gamma m_0 / \hbar = 1.99 \times 10^{-6}$ eV s/m. While the parameter α_{42} can be determined with the help of experiment data. According to a recent magnetotransport experiment in a 7.5 nm hole doped BP TF [27], the band gap E_g is 0.57 eV and the g_{zz}^* extracted from the Zeeman energy is 2.47. The overlap integral $\langle \varphi_v | \varphi_c \rangle$ can be obtained from the self-consistent calculation. The hole concentration n_h in the experimental sample ranges from 2.5 to 4.7 (in unit of 10^{12} cm $^{-2}$). We find that the overlap integral $\langle \varphi_v | \varphi_c \rangle$ is 0.9978, 0.9968, 0.994 for doping concentration 2.5, 3, 4 (in unit of 10^{12} cm $^{-2}$). Hence, we can safely take $\langle \varphi_v | \varphi_c \rangle$ as 0.996. According to the fact of these experimental data, we obtain that α_{42} is 3.86×10^{-7} eV s/m. Meanwhile, the band gap follows [19] $E_g^N = A/N^{0.73} + B$ with $A = 1.7$ eV, $B = 0.3$ eV for pristine BP TFs. It is worthwhile to note that Eq. (7) is also applicable to the effective single particle g factor of conduction band.

C. Exchange interaction enhancement on the g factor

In this section we evaluate the exchange interaction enhancement on the g factor via a screened Hartree-Fock approximation. We only evaluate the enhancement on g_{zz}^* which is the most interested component of the g factor tensor in BP TFs. The expression for the exchange interaction enhancement to the Landau level (LL) energy, calculated by using the wave functions $\Psi_{n,k_y}^{(\sigma)}(\mathbf{r}, z)$ is given by [32]

$$\begin{aligned} \Sigma_n^{(\sigma)} = & - \sum_{n', \sigma'} \sum_{k_y, k_y'} \int dz \int dz' \int d^2\mathbf{r} \int d^2\mathbf{r}' \\ & \times [\Psi_{n,k_y}^{(\sigma)}(\mathbf{r}, z)]^\dagger [\Psi_{n',k_y'}^{(\sigma')}(\mathbf{r}', z')]^\dagger V(\mathbf{r} - \mathbf{r}', z, z') \\ & \times \Psi_{n',k_y'}^{(\sigma')}(\mathbf{r}, z) \Psi_{n,k_y}^{(\sigma)}(\mathbf{r}', z'), \end{aligned} \quad (8)$$

where $V(\mathbf{r} - \mathbf{r}', z, z')$ is the Coulomb interaction potential donating the interaction between two point charges at (\mathbf{r}, z) and (\mathbf{r}', z') , and $\Psi_{n,k_y}^{(\sigma)}(\mathbf{r}, z)$ is the single particle states. The method to obtain $\Psi_{n,k_y}^{(\sigma)}(\mathbf{r}, z)$ is presented in Appendix B. Using the the Fourier transformation of the Coulomb potential

$$V(\mathbf{r} - \mathbf{r}', z, z') = \int \frac{d^2\mathbf{q}}{(2\pi)^2} K(q, z, z') e^{i\mathbf{q} \cdot (\mathbf{r} - \mathbf{r}')}, \quad (9)$$

the exchange interaction energy can be rewritten as

$$\begin{aligned} \Sigma_n^{(\sigma)} = & - \sum_{n', \sigma'} \sum_{k_y, k_y'} \int \frac{d^2\mathbf{q}}{(2\pi)^2} \int dz \int dz' \phi^{(\sigma)}(z) \phi^{(\sigma)}(z) \\ & \times \phi^{(\sigma)}(z') \phi^{(\sigma)}(z') J_{n,n'}^{\sigma, \sigma'}(\mathbf{q}) K(q, z, z') J_{n',n}^{\sigma', \sigma}(-\mathbf{q}), \end{aligned}$$

with

$$\begin{aligned} J_{n,n'}^{\sigma, \sigma'}(\mathbf{q}) = & \langle \Phi_{n,k_y}^{(\sigma)}(\mathbf{r}) | e^{i\mathbf{q} \cdot \mathbf{r}} | \Phi_{n',k_y'}^{(\sigma')}(\mathbf{r}) \rangle \\ = & \sum_{m, m'=0}^M (c_m^{v,n*} c_{m'}^{v,n'} + d_m^{v,n*} d_{m'}^{v,n'}) \langle m, k_y | e^{i\mathbf{q} \cdot \mathbf{r}} | m', k_y' \rangle, \end{aligned}$$

while $J_{n',n}^{\sigma', \sigma}(-\mathbf{q}) = \langle \Phi_{n',k_y'}^{(\sigma')}(\mathbf{r}') | e^{-i\mathbf{q} \cdot \mathbf{r}'} | \Phi_{n,k_y}^{(\sigma)}(\mathbf{r}') \rangle$ is similar to $J_{n,n'}^{\sigma, \sigma'}(\mathbf{q})$. The form factors $F_{mm'}(\mathbf{q}) = \langle m, k_y | e^{i\mathbf{q} \cdot \mathbf{r}} | m', k_y' \rangle$ for $m' \geq m$ case is

$$\begin{aligned} F_{mm'}(\mathbf{q}) = & \sqrt{\frac{m! 2^m}{m'! 2^{m'}}} (i\kappa q l_B)^{m'-m} e^{i(m'-m)\theta} L_m^{m'-m} \left(\frac{\kappa^2 q^2 l_B^2}{2} \right) \\ & \times e^{-\kappa^2 q^2 l_B^2 / 4} e^{i\kappa q_y (k_y + k_y') l_B^2 / 2} \delta_{k_y, k_y - q_y}, \end{aligned} \quad (10)$$

where $q = \sqrt{q_x^2 + q_y^2}$, $\theta = \arctan(q_x/q_y)$, and $L_n^\alpha(x)$ is the associate Laguerre polynomials. For $m' < m$ case, it can be determined by the identity $F_{mm'}(\mathbf{q}) = [F_{mm'}(-\mathbf{q})]^*$. Using the relations $\sum_{k_x} \rightarrow L_x L_y / 2\pi l_B^2$, $d^2\mathbf{q} = q dq d\theta$, finally, we obtain the exchange interaction correction energy as

$$\begin{aligned} \Sigma_n^{(\sigma)} = & - \sum_{n', \sigma'} v_{n'}^{(\sigma')} \int d\theta \int \frac{q dq}{(2\pi)^2} \int dz \int dz' |\phi^{(\sigma)}(z)|^2 \\ & \times J_{n,n'}^{\sigma, \sigma'}(\mathbf{q}) K(q, z, z') J_{n',n}^{\sigma', \sigma}(-\mathbf{q}) |\phi^{(\sigma)}(z')|^2, \end{aligned} \quad (11)$$

with

$$v_n^{(\sigma)} = 2\pi l_B^2 \int [1 - f(E_n^{(\sigma)})] D(E - E_n^{(\sigma)}) dE, \quad (12)$$

where $v_n^{(\sigma)}$ is the filling factor in the hole band as we mainly focus on the hole doped samples, and $D(E - E_n^{(\sigma)})$ is the density of states of each LL. In order to take into account the LL broadening arising from the random potential caused by defects and impurities in actual samples, we use a Gaussian profile for $D(E)$, which is given by $D(E) = \frac{1}{2\pi l_B^2 \sqrt{2\pi} \Gamma} e^{-\frac{E^2}{2\Gamma^2}}$.

We take the LL broadening as $\Gamma = \Gamma_0 \sqrt{B}$ to include the magnetic field dependent effect. On the other hand, the Fourier transform of the Coulomb potential is determined by the equation below:

$$\left(q^2 - \frac{\partial^2}{\partial z^2} \right) K(q, z, z') = -\frac{2\pi e^2}{\varepsilon} \delta(z - z'), \quad (13)$$

with the solution given by $K(q, z, z') = \frac{2\pi e^2}{\varepsilon q} e^{-q|z-z'|}$, where ε is the dielectric constant. Furthermore, to include the contribution of the spatial dispersion through the screening effect in the two-dimensional hole gas into the exchange interaction correction energy, we have to make a change as $K(q, z, z') \rightarrow K(q, z, z') / \tilde{\varepsilon}(q)$, where $\tilde{\varepsilon}(q)$ is the dielectric function. In the long-wave Thomas-Fermi approximation the two-dimensional hole gas dielectric function has the following form [32]:

$$\begin{aligned} \tilde{\varepsilon}(q) = & 1 + \sum_{n, \sigma} D(E_F - E_n^{(\sigma)}) \int dz \int dz' |\phi^{(\sigma)}(z)|^2 \\ & \times J_{n,n'}^{\sigma, \sigma'}(0) K(q, z, z') J_{n',n}^{\sigma', \sigma}(0) |\phi^{(\sigma)}(z')|^2. \end{aligned} \quad (14)$$

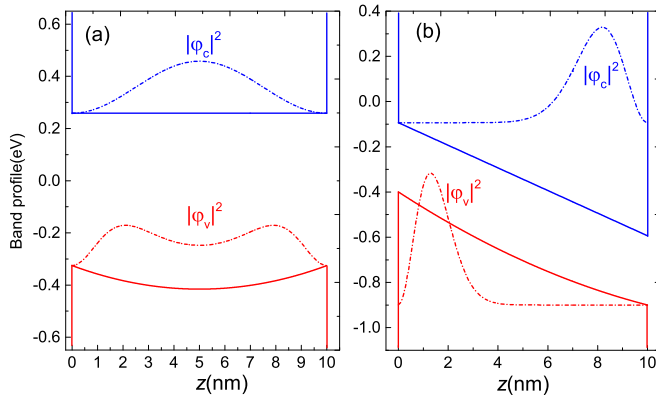


FIG. 2. Band profile and electron density for states in the conduction (blue lines) and valence (red lines) band obtained from self-consistent calculations for hole doping density $n_h = 5 \times 10^{12} \text{ cm}^{-2}$ with gate electric field (a) $E_z = 0$ and (b) $E_z = 0.5 \text{ MV/cm}$. The dielectric function $\epsilon = 10$ and temperature $T = 30 \text{ K}$. Notably, the density probabilities for electron and hole ground states are both positive and plotted schematically in the figure to describe the spatial distribution of electron and hole states in the BP thin film without and with external electric fields.

The energy of the LLs therefore has the form

$$\tilde{E}_n^{(\sigma)} = E_n^{(\sigma)} + \Sigma_n^{(\sigma)}, \quad (15)$$

with the exchange interaction taken into account. The effective g factor can be extracted from

$$g^* = \frac{|\tilde{E}_{n_F}^{(\uparrow)} - \tilde{E}_{n_F}^{(\downarrow)}|}{\mu_B B} = g_{zz}^* + \frac{|\Sigma_{n_F}^{(\uparrow)} - \Sigma_{n_F}^{(\downarrow)}|}{\mu_B B} = g_{zz}^* + g_{\text{ex}}, \quad (16)$$

where $\mu_B B$ is the spin splitting arising from Zeeman effect and g_{ex} is the exchange interaction enhanced g factor.

III. RESULTS AND DISCUSSIONS

In what follows, we will give some numerical examples and discussions on the band structure and the effective g factor for BP TFs. Figure 2 presents the band profile and electron density for states in conduction (blue lines) and valence (red lines) band for a 10 nm BP TF under hole doping density $n_h = 5 \times 10^{12} \text{ cm}^{-2}$ and $T = 30 \text{ K}$ (a) with and (b) without gate electric field. According to our calculations, only the first hole band is occupied. As shown in Fig. 2(a), we find that the build-in electric field arising from the doping pushes the holes to the two surfaces of TFs but the hole wave function still has a large overlap with the electron's. Here the band edges are adjusted to reproduce the estimated gap [19] ($E_c + \epsilon_c^1 - E_v - \epsilon_v^1 \approx 0.5$) of a 10 nm TF ($N \approx 20$). When a gate electric field $E_z = 0.5 \text{ MV/cm}$ is applied as depicted in Fig. 2(b), the energy gap remains $\sim 0.32 \text{ eV}$ due to the screening effect. However, the gate electrical field pushes the electrons and holes in opposite directions, leading to spatially separated electron and hole states. Meanwhile, we find that the free holes are mostly confined within few BP atomic layers at the surface, which is consistent with the recent experiment observation [23].

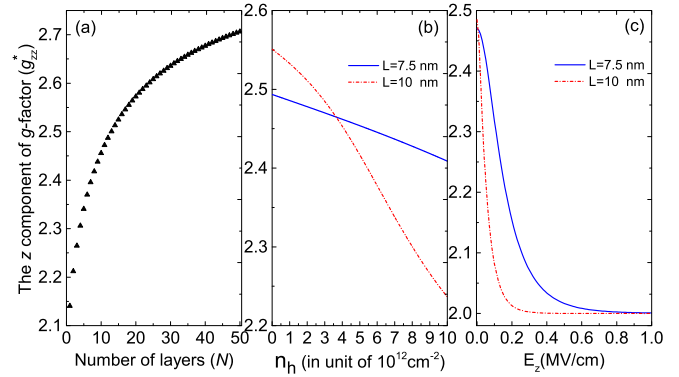


FIG. 3. (a) The z component of g factor (g_{zz}^*) in pristine BPTFs as a function of the number of layers; (b) the g_{zz}^* versus the hole doping concentration n_h under different BP thickness; (c) the g_{zz}^* versus the gate induced electric field E_z under hole doping concentration $n_h = 3 \times 10^{12} \text{ cm}^{-2}$ with different thickness. The blue solid (red dash-dotted) line represent the results for 7.5 (10) nm BP TF.

According to Eq. (7), we find that the effective single particle g factor in pristine BP TF is anisotropic arising from the anisotropic band structure with $g_{xx}^* \simeq g_{yy}^* \simeq 2.0$, and g_{zz}^* sensitively depend on the band gap and the interband coupling. The g_{zz}^* can be tuned by the sample thickness and the doping concentration as well as the gate electric field. Figure 3 presents the g_{zz}^* as functions of (a) the number of BP layers (N), (b) the hole doping concentration, and (c) the gate electric field. As shown in Fig. 3(a), we find that the g_{zz}^* in pristine BP TFs becomes larger when the number of BP layers increases because it minishes the band gap [19,38]. The g_{zz}^* in monolayer pristine BP equals 2.14 and approaches 2.90 when the sample is thick enough. The percentage change compared with the bare g factor in vacuum ranges from 7% to 45% with increasing BP thickness. From Fig. 3(b), we find that the g_{zz}^* decreases with increasing doping concentration since the doping induced build-in electric field pushes the holes to the two surfaces of the TFs which reduces the overlap integral ($\langle \varphi_v | \varphi_c \rangle$). However, this effect is inapparent when the sample thickness decreases [see the red dash-dotted line and the blue solid line in Fig. 3(b)] since the overlap integral becomes larger with decreasing BP thickness under the same doping density. Consequently, for the ultrathin (monolayer) limit, we can safely conclude that the g_{zz}^* is nearly unaffected by the doping density. Likewise, the gate electric field has similar effect on g_{zz}^* with that of doping because both of them reduce the overlap integral. However, the effect induced by the gate electric field manifest is more apparent. As presented in Fig. 3(c), the g_{zz}^* declines with the gate electric field E_z dramatically for both 7.5 and 10 nm thick BP TFs. The reason is that the gate electric field pushes the electrons and holes in opposite directions [see Fig. 2(b)], which minishes the overlap integral significantly. For relatively large gate electric field, i.e., $E_z > 0.8 \text{ MV/cm}$, the g_{zz}^* approaches 2.0 due to the spatially separated electrons and holes [see Fig. 2(b)] which contribute to negligible interband coupling. In this case we have $g_{xx}^* \approx g_{yy}^* \approx g_{zz}^* = g_0$ which means that the effective single-particle g factor in BP TF is isotropic.

Figure 4 presents (a) the exchange interaction enhanced g factor g_{ex} and (b) the effective g factor g^* as a function of

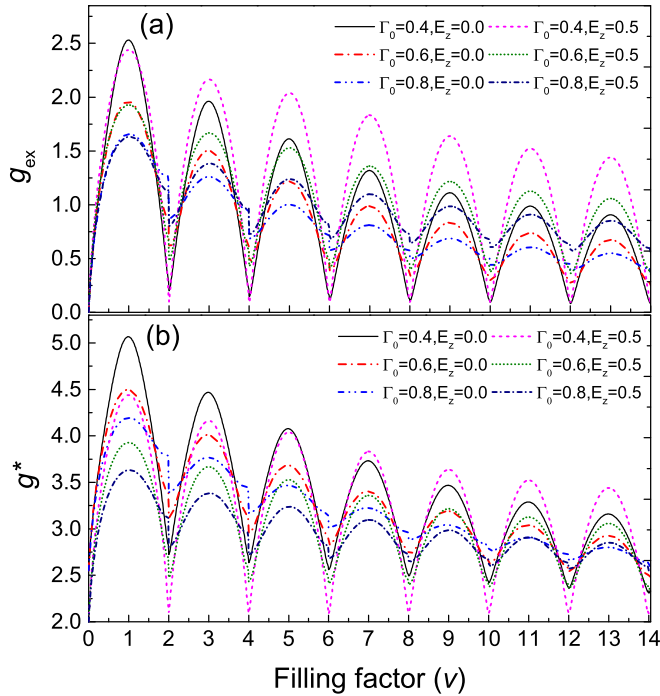


FIG. 4. (a) The exchange interaction enhancement on the g factor g_{ex} and (b) the effective g factor g^* as a function of filling factor ν (hole doping concentration $n_h = eB/h$) under magnetic field $B = 30$ T for different LL broadenings width $\Gamma = \Gamma_0\sqrt{B}$ meV with and without electric field E_z (in unit of MV/cm).

filling factor (hole doping density) under a fixed magnetic field $B = 30$ T for different LL broadenings Γ with and without gate electric field E_z . As shown in Fig. 4(a), we find that the g_{ex} shows maxima at the Fermi level for odd values of the LL filling factor, arising from the maximal difference of the hole concentrations with opposite spins $|n_{\uparrow} - n_{\downarrow}|$. However, the hole numbers with opposite spin at even filling factors are almost the same, leading to the minimum enhancement to the g factor because of the minimum $|n_{\uparrow} - n_{\downarrow}|$, which is similar to that in conventional two-dimensional (2D) electron gas [32,33]. The g_{ex} decreases with increasing LL broadening Γ since larger LL broadening heightens the screening effect and reduces the difference of hole numbers with opposite spins. When a gate electric field is applied, the holes are pushed into only one side of the sample located at about three atomic BP layers [see the $|\varphi_v|^2$ shown in Fig. 2(b)]. In consequence, compared with the zero electric field case, the distance of the holes are reduced and therefore the Coulomb interaction is enhanced, leading to a larger g_{ex} for the same LL broadening. From Fig. 4(b) we find that the behavior of the effective g factor g^* ($=g_{\text{zz}}^* + g_{\text{ex}}$) is similar to that of g_{ex} . However, the gate electric field has dual influence on g^* . On one hand, the gate electric field minishes the g_{zz}^* via reducing the overlap integral. On the other band, it enlarges the g_{ex} via decreasing the distances of the holes which contributes to enhanced Coulomb interaction. Hence, we find crosses in the g^* for finite gate electric field and the zero case for the same LL broadenings.

Figure 5 displays (a) the exchange interaction enhanced g factor g_{ex} and (b) the effective g factor g^* as a function

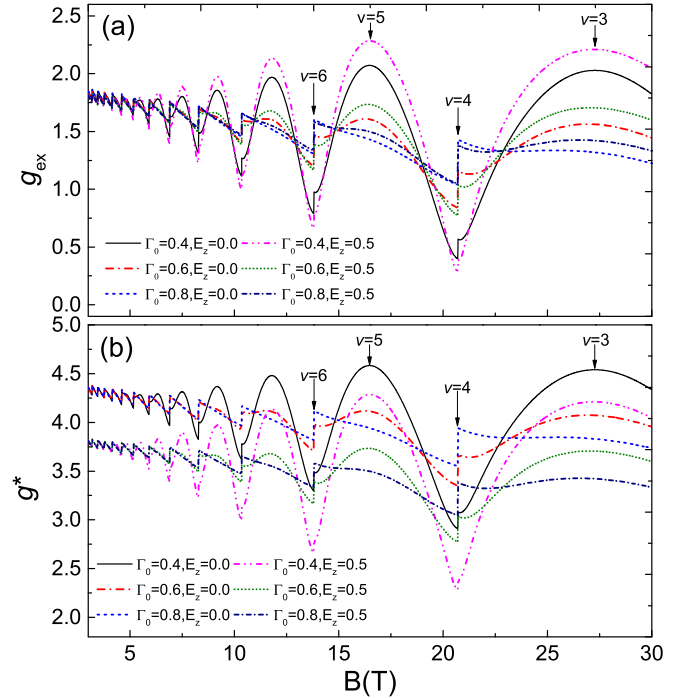


FIG. 5. (a) The exchange interaction enhancement on the g factor g_{ex} and (b) the effective g factor g^* as a function of magnetic field B when the hole doping density is 2.0×10^{12} cm $^{-2}$ for different LL broadenings $\Gamma = \Gamma_0\sqrt{B}$ meV with and without electric field E_z (in unit of MV/cm).

of magnetic field under hole doping density 2.0×10^{12} cm $^{-2}$ for different LL broadenings Γ with and without gate electric field E_z . As illustrated in Fig. 5(a), when the magnetic field increases, the degeneracy of each LLs lifts by Zeeman splitting, and the Fermi level shifts from the paired spin split LLs one by one. Therefore, we find that the g_{ex} oscillates with the magnetic field and shows maxima (minima) at odd (even) filling factors. The g_{ex} sensitively depends on the LL broadening Γ since it affects the screening effect [see Eq. (14)] and the difference of the hole numbers between opposite spins $|n_{\uparrow} - n_{\downarrow}|$. Notably, we observe that the g_{ex} factor becomes nearly a constant (see the blue dashed and navy dash-dotted lines) for relatively large LL broadening because the Zeeman gap is nearly quenched in this circumstance. We believe that the constant g_{ex} is more close to the experiment data since the broadening of photoluminescence (PL) spectra is about 20 meV [39], which implies that there are a large number of defects and impurities in the sample. And this will result in a large LL broadening. When a gate electric field is applied, the holes are pushed into only one side of the sample which minishes the distance of the holes [see the $|\varphi_v|^2$ shown in Fig. 2(b)]. Consequently, the Coulomb interaction is enhanced which leads to a larger g_{ex} for the same LL broadening compared with that of zero gate electric field case. From Fig. 5(b) we find that the g^* break into two branches arising from different g_{zz}^* under zero and finite gate electric field. The g_{zz}^* is 2.51 and 2.0, respectively, corresponding to E_z equal to 0 and 0.5 MV/cm. Other features of the g^* is similar with that of the g_{ex} .

IV. SUMMARY

In summary, we theoretically studied the effective g factor in the BP TFs based on a multiband $\mathbf{k} \cdot \mathbf{p}$ theory. We demonstrated that the effective single particle g factor in pristine BP TF is anisotropic arising from its anisotropic band structure with $g_{xx}^* \approx g_{yy}^* \approx 2.0$ and g_{zz}^* sensitively depending on the interband coupling and band gap. The g_{zz}^* in pristine BP ranges from 2.14 to 2.9 as the BP thickness increases from monolayer to bulk. It approaches 2.0 with increasing hole doping density and gate electric field since both of them minish the interband coupling by reducing the overlap integral between the electron and hole wave functions. We also estimated the exchange interaction enhancement on the effective single particle g factor by using the screened Hartree-Fock approximation. The exchange interaction enhanced g factor (g_{ex}) shows maxima (minima) at odd (even) filling factors. The effective g factor (g^*) oscillates with increasing magnetic fields and sensitively depends on the Landau level broadening as well as the gate electric field because both of them affect the interband coupling and electron-electron interaction.

ACKNOWLEDGMENTS

This work was supported by the NSFC (Grants No. 61674145, No. 11434010, No. 11574303, No. 11304306, No. 61290303, No. 11274108, and No. 11374002) and Grant No. 2015CB921503 from the MOST of China.

APPENDIX A

In this Appendix we present the detail derivation for the effective single particle g factor. Within the $\mathbf{k} \cdot \mathbf{p}$ framework, the Schrödinger equation can be expressed as [40,41]

$$\sum_{n'} \left(\sum_{\alpha\beta} D_{nn'\alpha\beta} k_\alpha k_\beta - E \delta_{nn'} \right) \psi_{n'} = 0, \quad (\text{A1})$$

where the Hamiltonian matrix element coefficients are given by

$$D_{nn'\alpha\beta} = \frac{\hbar^2}{2m_0} \delta_{nn'} \delta_{\alpha\beta} + \frac{\hbar^2}{m_0} \sum_l \frac{P_{n,l}^\alpha P_{l,n}^\beta}{E_n^{(0)} - E_l^{(0)}}, \quad (\text{A2})$$

with $\mathbf{P} = \mathbf{p} + \frac{\hbar}{4m_0c^2} (\boldsymbol{\sigma} \times \nabla V)$, $P_{n,l}^\alpha = \langle n | P_\alpha | l \rangle$, $P_{l,n}^\beta = \langle l | P_\beta | n \rangle$, where $|n\rangle$ is the Bloch state corresponding to the n th band $E_n^{(0)}$. The sum index l runs over all the Bloch bands except the n th. Hence, the secular equation can be written as

$$\sum_{n'} \left(\sum_{\alpha\beta} \frac{1}{2} [D_{nn'\alpha\beta}^S \{k_\alpha, k_\beta\} + D_{nn'\alpha\beta}^A [k_\alpha, k_\beta]] - E \delta_{nn'} \right) \psi_{n'} = 0, \quad (\text{A3})$$

where $D_{nn'\alpha\beta}^S$ and $D_{nn'\alpha\beta}^A$ are the symmetric and asymmetric part of $D_{nn'\alpha\beta}$ (i.e., $D_{nn'\alpha\beta}^S = (D_{nn'\alpha\beta} + D_{nn'\beta\alpha})/2$ and $D_{nn'\alpha\beta}^A = (D_{nn'\alpha\beta} - D_{nn'\beta\alpha})/2$), respectively. $[k_\alpha, k_\beta]$ and $\{k_\alpha, k_\beta\}$ are commutator and anticommutator, respectively.

$D_{nn'\alpha\beta}^S$ can be written as

$$D_{nn'\alpha\beta}^S = \frac{\hbar^2}{2m_0} \left(\delta_{nn'} \delta_{\alpha\beta} + \sum_l \frac{P_{n,l}^\alpha P_{l,n'}^\beta + P_{n,l}^\beta P_{l,n'}^\alpha}{E_n^{(0)} - E_l^{(0)}} \right), \quad (\text{A4})$$

and the antisymmetric part $D_{nn'\alpha\beta}^A$ is given by

$$D_{nn'\alpha\beta}^A = \frac{\hbar^2}{2m_0} \sum_l \frac{P_{n,l}^\alpha P_{l,n'}^\beta - P_{n,l}^\beta P_{l,n'}^\alpha}{E_n^{(0)} - E_l^{(0)}}. \quad (\text{A5})$$

When the system is subjected to a magnetic field, the secular equation becomes

$$\sum_{n'} \left(\sum_{\alpha\beta} \frac{1}{2} [D_{nn'\alpha\beta}^S \{k_\alpha, k_\beta\} + D_{nn'\alpha\beta}^A [k_\alpha, k_\beta]] + \mu_B \boldsymbol{\sigma} \cdot \mathbf{B} - E \delta_{nn'} \right) \psi_{n'} = 0, \quad (\text{A6})$$

where the Bohr magneton $\mu_B = |e|\hbar/2m_0$, $[k_\alpha, k_\beta] = \varepsilon_{\alpha\beta\gamma} e B_\gamma / i\hbar$, and $\varepsilon_{\alpha\beta\gamma}$ is the Levi-Civita symbol. We consider an external magnetic field applied along z axis. The momentum \mathbf{p} is now replaced by the canonical momentum $\mathbf{p} \rightarrow \mathbf{p} + e\mathbf{A}$, where $\mathbf{A} = B(-y, x, 0)/2$ is the vector potential adopting the symmetry gauge. In this case, $[k_\alpha, k_\beta] = 2m_0\mu_B B / i\hbar^2$, the secular equation becomes

$$\sum_{n'} \left(\mu_B \frac{\hbar^2}{2im_0} \sum_l \frac{P_{n,l}^\alpha P_{l,n'}^\beta - P_{n,l}^\beta P_{l,n'}^\alpha}{E_n^{(0)} - E_l^{(0)}} B_z + \mu_B m_s B_z + \sum_{\alpha\beta} \frac{1}{2} D_{nn'\alpha\beta}^S \{k_\alpha, k_\beta\} - E \delta_{nn'} \right) \psi_{n'} = 0, \quad (\text{A7})$$

then we obtain the analytical form of the effective magnetic moment of the electron in a crystal:

$$\mu = \mu_B \left[\delta_{\alpha\beta} + \frac{1}{im_0} \sum_l \frac{P_{n,l}^\alpha P_{l,n}^\beta - P_{n,l}^\beta P_{l,n}^\alpha}{E_n^{(0)} - E_l^{(0)}} \right]. \quad (\text{A8})$$

Hence, the components of the g factor tensor $g = 2\mu/\mu_B$ is given by

$$g_{\alpha\beta}^* = g_0 \left[\delta_{\alpha\beta} + \frac{1}{im_0} \sum_l \frac{P_{n,l}^\alpha P_{l,n}^\beta - P_{n,l}^\beta P_{l,n}^\alpha}{E_n^{(0)} - E_l^{(0)}} \right], \quad (\text{A9})$$

which is just the analytical expressions of the effective single particle g factor tensor in Eq. (5).

APPENDIX B

To estimate the influence of the exchange interaction on the effective single particle g factor of BP TF under a perpendicular magnetic field, we first have to calculate the 2D electron spectrum in the absence of exchange interaction, i.e., the single particle states. In this Appendix we present the derivation of the single particle state $\Psi_{n,k_y}^{(\sigma)}(\mathbf{r}, z)$. In this case, the Hamiltonian for the system turns into $H_{\text{TF}} = H_{k_{\parallel}} + H_z + H_{k_z}$, where $H_z = \frac{1}{2} g_{zz}^* \sigma \mu_B B$ is the Zeeman energy with g_{zz}^* the single particle g factor calculated in Sec. II B, $\sigma = \pm 1$ donates spin up and down, respectively. Owing to the strong confinement of perpendicular magnetic field, we can decouple the motion of electron in the x - y plane and the z direction. We have solved the z dependent part of Hamiltonian H_{TF} self-consistently and obtained the subbands with the corresponding

wave functions $\varphi_j(z)$ in Sec. II B. Here we only need to focus on the in-plane part.

When a perpendicular magnetic field $\mathbf{B} = (0, 0, B)$ is applied, taking Landau gauge $\mathbf{A} = (0, Bx, 0)$ and defining the creation operators as $\hat{a} = \sqrt{\frac{m_{cx}\omega_c}{2\hbar}}(x + x_0 + i\frac{p_x}{m_{cx}\omega_c})$, we find that the in-plane part Hamiltonian $H_{k_{\parallel}}$ turns into

$$H_{k_{\parallel}} = \begin{pmatrix} H_c & H_{cv} \\ H_{cv}^* & H_v \end{pmatrix}, \quad (\text{B1})$$

where $H_c = E_c^j + (\hat{a}^\dagger \hat{a} + \frac{1}{2})\hbar\omega_c + \frac{1}{2}g_{zz}^* \sigma \mu_B B$, $H_v = E_v^j - (\hat{a}^\dagger \hat{a} + \frac{1}{2})\hbar\omega_v + (\hat{a}^2 + \hat{a}^{\dagger 2})\hbar\omega' + \frac{1}{2}g_{zz}^* \sigma \mu_B B$, $H_{cv} = \hbar\omega_\gamma(\hat{a} + \hat{a}^\dagger)$, $\omega_c = 2\sqrt{\alpha_c \beta_c}/l_B^2$ is the cyclotron frequency, $x_0 = l_B^2 k_y$ is the cyclotron center, and $l_B = \sqrt{\hbar/eB}$ is the magnetic length, $E_{c/v}^j$ are the thickness dependent subband edges which can be determined by the self-consistent calculations $\omega_\gamma = \gamma r_{xy}/\sqrt{2}\hbar l_B$, $\omega_v = (r_x + r_y)\omega_c$, $\omega' = (r_x - r_y)\omega_c/2$, with $r_{xy} = (\beta_c/\alpha_c)^{1/4}$, $r_x = \alpha_v/2\alpha_c$, and $r_y = \beta_v/2\beta_c$. The eigenvalues and eigenvectors can be evaluated numerically by taking the eigenvectors $|n, k_y\rangle$ of the number operator

$\hat{n} = \hat{a}^\dagger \hat{a}$ as the basis functions. In real space representation, $\langle x|n, k_y\rangle = \frac{e^{iky}}{\sqrt{L_x}} \phi_n[\kappa(x + x_0)/l_B]$, $\phi_n[\kappa(x + x_0)/l_B]$ are the wave functions of one-dimensional harmonic oscillator with cyclotron center x_0 and $\kappa = 1/r_{xy}$. Therefore, the in-plane part wave function of the system can be expressed as

$$\Phi_{j,n,k_y}^{(\sigma)}(x, y) = \sum_{m=0}^M \begin{pmatrix} c_m^n \\ d_m^n \end{pmatrix} |m, k_y\rangle, \quad (\text{B2})$$

where n is the Landau level (LL) index and j is the subband index. Throughout the paper, we only focus on the LLs belong to the first hole subband of BP TFs. The index j for wave functions and matrix elements of different operators will be omitted. Combining with the wave functions of the z direction, we obtain the wave function of the system $\Psi_{n,k_y}^{(\sigma)}(\mathbf{r}, z)$ given by

$$\Psi_{n,k_y}^{(\sigma)}(\mathbf{r}, z) = \varphi^{(\sigma)}(z) \Phi_{n,k_y}^{(\sigma)}(x, y). \quad (\text{B3})$$

Under the help of the above wave functions, we can calculate the exchange interaction enhancement to the LL energy and extract the enhanced g factor from it.

-
- [1] L. Li, Y. Yu, G. Ye, Q. Ge, X. Ou, H. Wu, D. Feng, X. H. Chen, and Y. Zhang, *Nat. Nanotech.* **9**, 372 (2014).
- [2] H. Liu, A. T. Neal, Z. Zhu, Z. Luo, X. Xu, D. Tománek, and P. D. Ye, *ACS Nano* **8**, 4033 (2014).
- [3] St. P. Koenig, R. A. Doganov, H. Schmidt, A. H. Castro Neto, and B. Özyilmaz, *Appl. Phys. Lett.* **104**, 103106 (2014).
- [4] A. S. Rodin, A. Carvalho, and A. H. Castro Neto, *Phys. Rev. Lett.* **112**, 176801 (2014).
- [5] T. Nishii, Y. Maruyama, T. Inabe, and I. Shirovani, *Synth. Met.* **18**, 559 (1987).
- [6] Fengnian Xia, Han Wang, and Yichen Jia, *Nat. Commun.* **5**, 4458 (2014).
- [7] C. Q. Han, M. Y. Yao, X. X. Bai, L. Miao, F. Zhu, D. D. Guan, S. Wang, C. L. Gao, C. Liu, D. Qian, Y. Liu, and J.-f. Jia, *Phys. Rev. B* **90**, 085101 (2014).
- [8] A. Castellanos-Gomez, L. Vicarelli, E. Prada, J. O. Island, K. L. Narasimha-Acharya, S. I. Blanter, D. J. Groenendijk, M. Buscema, G. A. Steele, J. V. Alvarez, H. W. Zandbergen, J. J. Palacios, and H. S. J. van der Zant, *2D Mater.* **1**, 025001 (2014).
- [9] A. Castellanos-Gomez, *J. Phys. Chem. Lett.* **6**, 4280 (2015).
- [10] X. Ling, H. Wang, S. Huang, F. Xia, and M. S. Dresselhaus, *PNAS* **112**, 4523 (2015).
- [11] Jingsi Qiao, Xianghua Kong, Zhi-Xin Hu, Feng Yang, and Wei Ji, *Nat. Commun.* **5**, 4475 (2014).
- [12] W. Lu, H. Nan, J. Hong, Y. Chen, C. Zhu, Z. Liang, X. Ma, Z. Ni, C. Jin, and Z. Zhang, *Nano. Res.* **7**, 853 (2014).
- [13] X. Wang, A. M. Jones, K. L. Seyler, V. Tran, Y. Jia, H. Zhao, H. Wang, L. Yang, X. Xu, and F. Xia, *Nat. Nanotech.* **10**, 517 (2015).
- [14] M. Buscema, D. J. Groenendijk, S. I. Blanter, G. A. Steele, H. S. J. van der Zant, and A. Castellanos-Gomez, *Nano. Lett.* **14**, 3347 (2014).
- [15] M. Engel, M. Steiner, and P. Avouris, *Nano. Lett.* **14**, 6414 (2014).
- [16] R. Fei, V. Tran, and L. Yang, *Phys. Rev. B* **91**, 195319 (2015).
- [17] Y. Jiang, R. Roldán, F. Guinea, and T. Low, *Phys. Rev. B* **92**, 085408 (2015).
- [18] T. Low, A. S. Rodin, A. Carvalho, Y. Jiang, H. Wang, F. Xia, and A. H. Castro Neto, *Phys. Rev. B* **90**, 075429 (2014).
- [19] V. Tran, R. Soklaski, Y. Liang, and L. Yang, *Phys. Rev. B* **89**, 224514 (2014).
- [20] X. Y. Zhou, R. Zhang, J. P. Sun, Y. L. Zou, D. Zhang, W. K. Lou, F. Cheng, G. H. Zhou, F. Zhai, and K. Chang, *Sci. Rep.* **5**, 12295 (2015).
- [21] X. Zhou, W.-K. Lou, F. Zhai, and K. Chang, *Phys. Rev. B* **92**, 165405 (2015).
- [22] R. Zhang, X. Y. Zhou, D. Zhang, W. K. Lou, F. Zhai, and K. Chang, *2D Mater.* **2**, 045012 (2015).
- [23] L. Li, F. Yang, G. J. Ye, Z. Zhang, Z. Zhu, W.-K. Lou, L. Li, K. Watanabe, T. Taniguchi, K. Chang, Y. Wang, X. H. Chen, and Y. Zhang, *Nat. Nanotech.* **11**, 593 (2016).
- [24] L. Li, G. J. Ye, V. Tran, R. Fei, G. Chen, H. Wang, J. Wang, K. Watanabe, T. Taniguchi, L. Yang, X. H. Chen, and Y. Zhang, *Nat. Nanotech.* **10**, 608 (2015).
- [25] X. Chen, Y. Wu, Z. Wu, S. Xu, L. Wang, Y. Han, W. Ye, T. Han, Y. He, Y. Cai, and N. Wang, *Nat. Commun.* **6**, 7315 (2015).
- [26] V. Tayari, N. Hemsworth, I. Fasih, A. Favron, E. Gaufres, G. Gervais, R. Martel, and T. Szkopek, *Nat. Commun.* **6**, 7702 (2015).
- [27] G. Long, D. Maryenko, J. Y. Shen, S. G. Xu, J. Q. Hou, Z. F. Wu, W. K. Wong, T. Y. Han, J. X. Z. Lin, Y. Cai, R. Lortz, and N. Wang, *2D Mater.* **3**, 031001 (2016).
- [28] Y. Cao, A. Mishchenko, G. Yu, K. Khestanova, A. Rooney, E. Prestat, A. Kretinin, P. Blake, M. Shalom, G. Balakrishnan, I. V. Grigorieva, K. S. Novoselov, B. A. Piot, M. Potemski, K. Watanabe, T. Taniguchi, S. J. Haigh, A. K. Geim, and R. V. Gorbachev, *Nano Lett.* **15**, 4914 (2015).
- [29] N. Gillgren, D. Wickramaratne, Y. Shi, T. Espiritu, J. Yang, J. Hu, J. Wei, X. Liu, Z. Mao, K. Watanabe, T. Taniguchi, M. Bockrath, Y. Barlas, R. K. Lake, and C. N. Lau, *2D Mater.* **2**, 011001 (2015).

- [30] A. Malinowski and R. T. Harley, *Phys. Rev. B* **62**, 2051 (2000).
- [31] R. Kotlyar, T. L. Reinecke, M. Bayer, and A. Forchel, *Phys. Rev. B* **63**, 085310 (2001).
- [32] S. S. Krishtopenko, V. I. Gavrilenko, and M. Goiran, *J. Phys. Condens. Matter* **23**, 385601 (2011).
- [33] T. Ando and Y. Uemura, *J. Phys. Soc. Jpn.* **37**, 1044 (1974).
- [34] F. Stern, *Phys. Rev. Lett.* **18**, 546 (1967).
- [35] F. Stern, *Phys. Rev. B* **5**, 4891 (1972).
- [36] P. K. Li and I. Appelbaum, *Phys. Rev. B* **90**, 115439 (2014).
- [37] A. N. Rudenko and M. I. Katsnelson, *Phys. Rev. B* **89**, 201408(R) (2014).
- [38] A. N. Rudenko, S. Yuan, and M. I. Katsnelson, *Phys. Rev. B* **92**, 085419 (2015).
- [39] L. Li, J. Kim, C. Jin, G. Ye, D. Y. Qiu, F. H. da Jornada, Z. Shi, L. Chen, Z. Zhang, F. Yang, K. Watanabe, T. Taniguchi, W. Ren, S. G. Louie, X. Chen, Y. Zhang, and F. Wang, *Nat. Nanotech.* (2016), doi:[10.1038/NNANO.2016.171](https://doi.org/10.1038/NNANO.2016.171).
- [40] R. Winkler, *Spin-Orbit Coupling Effects in Two-Dimensional Electron and Hole Systems* (Springer, Berlin, 2003).
- [41] M. S. Dresselhaus, G. Dresselhaus, and A. Jorio, *Group Theory Application to the Physics of Condensed Matter* (Springer, Berlin, 2008).